Journal of Nuclear Materials 484 (2017) 236–244

Contents lists available at ScienceDirect

Journal of Nuclear Materials

journal homepage: www.elsevier.com/locate/jnucmat

The role of grain size in He bubble formation: Implications for swelling resistance

O. El-Atwani [a, *], J.E. Nathaniel II [a], A.C. Leff [a], B.R. Muntifering [b], J.K. Baldwin [c], K. Hattar [b], M.L. Taheri [a, **]

[a] Drexel University, Department of Materials Science & Engineering, Philadelphia, PA, USA
[b] Department of Radiation Solid Interactions, Sandia National Laboratories, NM, USA
[c] Center for Integrated Nanotechnologies, Los Alamos National Laboratory, Los Alamos, NM, USA

ARTICLE INFO

Article history:
Received 18 August 2016
Received in revised form
28 November 2016
Accepted 2 December 2016
Available online 7 December 2016

Keywords:
Bubble formation
Nanocrystalline
Denuded zone
Swelling

ABSTRACT

Nanocrystalline metals are postulated as radiation resistant materials due to their high defect and particle (e.g. Helium) sink density. Here, the performance of nanocrystalline iron films is investigated in-situ in a transmission electron microscope (TEM) using He irradiation at 700 K. Automated crystal orientation mapping is used in concert with in-situ TEM to explore the role of grain orientation and grain boundary character on bubble density trends. Bubble density as a function of three key grain size regimes is demonstrated. While the overall trend revealed an increase in bubble density up to a saturation value, grains with areas ranging from 3000 to 7500 nm^2 show a scattered distribution. An extrapolated swelling resistance based on bubble size and areal density indicated that grains with sizes less than 2000 nm^2 possess the greatest apparent resistance. Moreover, denuded zones are found to be independent of grain size, grain orientation, and grain boundary misorientation angle.

Published by Elsevier B.V.

1. Introduction

Material degradation at high radiation doses [1] and the extreme irradiation environments such as those that occur in fission and fusion energy systems occurs via the nucleation of defects. These include bubbles, voids, and dislocation loops that alter the properties of the irradiated materials [2–7] and ultimately decrease performance [3]. Such degradation occurs in both fusion and fission materials. For example, in tungsten, of interest in fusion, damage from He ions can produce morphological changes [8–10] that cause enhanced erosion that can eventually degrade the plasma performance through radiation cooling [11]. Similarly, fission materials exposed to neutron irradiation and fission fragments can degrade through swelling, embrittlement, and hardening [3,5]. Nanocrystalline materials with their improved mechanical properties are more tolerant to high radiation doses [12–14]. Their increased grain boundary population translates to an increased defect sink density that could enhance irradiation induced defect annihilation [15–18].

Grain boundaries, acting as defect sinks [19–21], may assist in suppressing or controlling radiation damage [22]. Consequently, it has been speculated that a high grain boundary density could increase the irradiation dose threshold necessary to accumulate a high enough density of defects to significantly change the properties of the material [23]. Several experimental and theoretical studies have investigated the performance of ultrafine grained and nanocrystalline materials with respect to dislocation loop, bubble, and void densities [16–18,24–40], as well as morphological instabilities such as nanostructure formation [10,23,41]. In several metals (Copper [29], Nickel [29] and Gold [30]), nanocrystalline microstructures have exhibited higher radiation tolerance than coarse grained microstructures as measured by irradiation induced cluster defect density. Similarly, regarding bubble formation and evolution in BCC nanocrystalline materials, it has been demonstrated experimentally [17] that nanocrystalline tungsten grains lead to lower helium bubble density in the grain matrix when compared to ultrafine grains. This observation is in agreement with simulations performed by Sefta *et al.* [39], which demonstrated higher helium retention in bicrystalline tungsten materials compared to single crystalline tungsten. Molecular dynamics

* Corresponding author.Materials Science and Technology Division, Los Alamos National Laboratory, Los Alamos, NM, USA
** Corresponding author.
E-mail address: oelatwan25@gmail.com (O. El-Atwani).

http://dx.doi.org/10.1016/j.jnucmat.2016.12.003
0022-3115/Published by Elsevier B.V.

simulations performed by Refs. [16,19,24–26,42] demonstrated the role of grain boundaries in annihilating interstitial defects and vacancies. Bai *et al.* [25] demonstrated an enhanced defect annihilation process through rapid interstitial defect absorption and reemission (and subsequent combination) with vacancies approaching grain boundaries. A large scatter of defect densities as a function of grain size has been observed, however, which has been attributed to the dependence of boundary sink efficiency on grain boundary character [27] and other interfacial deviations [43].

Experimental evidence of the dependence of bubble formation and swelling due to helium implantation on grain size is crucial in investigating the performance of candidate nanocrystalline materials for future nuclear applications and the development of mesoscale predictive models. When displacement energies are sufficient to produce vacancies that bind to helium in stable helium-vacancy complexes, this occurs in timescales as short as hundreds of picoseconds [44]. For example, in pure iron at intermediate temperatures (> 573 K) small vacancy clusters formed by migration of individual vacancies are unstable [45] and need helium to stabilize them. The growth of these helium-vacancy clusters lead to bubble formation that degrades mechanical properties [46,47]. Interstitial helium atoms, due to their low migration energy (0.06 eV) [48], are predicted to agglomerate quickly and eject interstitial Fe atoms, eventually leading to the formation of helium-vacancy clusters, and eventually bubbles. Small helium-vacancy clusters are also mobile at temperatures over 573 K [45] and therefore, their coalescence can enhance bubble formation. The relationship between bubble formation and grain size are relatively unknown, especially in nanocrystalline size regimes.

In this work, nanocrystalline Fe is used as a model BCC material to investigate the performance of high sink density materials under helium irradiation in-situ in the transmission electron microscope (TEM), coupled with automated crystal orientation mapping (ACOM) [49] for grain orientation analysis. A comparison of bubble densities in nanocrystalline to ultrafine grained size regimes shows that bubble density increases with grain size in the nanocrystalline regime, but scatters in the transition from the nanocrystalline to the ultrafine grained regime; this appears to reach a saturation value in the ultrafine grained regime. An apparent swelling, as extrapolated from the bubble density and size data, is shown to follow similar grain size trends, as expected. These results suggest that nanocrystalline materials have potential for use in extreme environments where swelling due to void or bubble formation is a concern.

2. Experimental

2.1. Sample preparation

Nanocrystalline Fe films (approximately 100 nm nominal thickness) [50,51] were sputter-deposited on NaCl substrates. The details of the film preparation conditions are described elsewhere by Vetterick *et al.* [50]. The films were then floated in water onto 300 mesh molybdenum TEM grids (Tedpella, Inc.) and annealed to 873 K in-situ in a JEOL 2100 LaB_6 TEM using a Gatan 628 single-tilt heating stage to reach an equilibrium microstructure. The overall microstructure consists of both nanocrystalline (<100 nm diameter) and ultrafine (100–500 nm diameter) grains. The supplemental material briefly describes the calculation of the average grain size.

2.2. Irradiation and microstructural characterization

In-situ TEM irradiation with He was performed using the In-situ Ion Irradiation TEM facility [52] at Sandia National Laboratories with He ions at 700 K and a dose rate of 8.74×10^{17} He/m^2-s^- to 2.8×10^{21} He/m^2. The Monte Carlo computer code Stopping Range of Ions in Matter (SRIM) (version 2013) [53] was used to perform analysis to determine the distribution of damage introduced into the materials (Fig. 1). The mean ion range in the depth direction is approximately 35 nm for 10 keV He^+ irradiation at 60° incidence, which implies that the He ions will remain implanted in the sample rather than being transmitted through it. Assuming 40 eV as a displacement damage energy threshold [54] and a 100 nm-film thickness, the detailed calculation with full damage cascades option in SRIM demonstrated an average vacancy production of approximately 31 vacancies/ion. The final helium concentration, using a maximum implanted depth of 80 nm as shown in Fig. 1 is then found to be 3.5×10^{28} m^{-3} and the He/Fe atoms ratio is approximately 0.41 (in the implanted region). At peak depth (35 nm) as shown in Fig. 1 the vacancy production was predicted to be 0.38 vacancies/ion/nm and the corresponding damage value was approximately 12.5 dpa.

He bubble density, location, and morphology were characterized using bright-field TEM imaging in a JEOL 2100 LaB_6 TEM at under-focused (bubbles appears bright) and over-focused (bubbles appear dark) conditions and Fresnel imaging conditions plus additional ACOM analysis [55]. ACOM was performed with the NanoMEGAS ASTAR precession electron diffraction system [49], using a 10 nm spot size and a 2 nm step size.

A total of 32 grains from three separate regions on the film were quantified using under-focused and over-focused bright-field images. For orientation analysis, index values ranged from 172 to 1100 and grains that indexed with a reliability of less than 20 were ignored. An example of an inverse pole-figure (IPF) map with the corresponding index and reliability maps produced using the NanoMEGAS ASTAR system is given in the supplemental section.

To determine bubble areal density, several 15 nm diameter circles were drawn randomly on each grain using ImageJ software [56]. The number of bubbles in each circle were counted and the density distribution was taken. Bubble areas were estimated by drawing a circle with ImageJ software around the perimeter of bubbles chosen randomly on every grain and an average area taken. To eliminate errors in grain size calculations due to differences in grain morphologies, the bubble density and bubble diameter graphs are plotted as a function of projected grain area. It should be

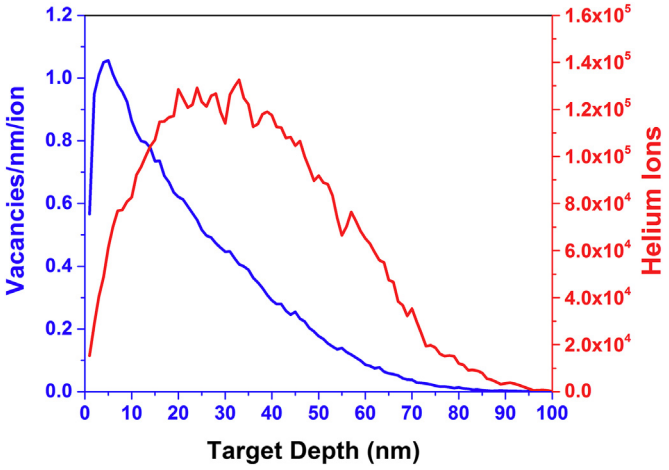

Fig. 1. SRIM calculations performed for 10 keV helium ions bombarding 100 nm iron sample at 60° incidence to the ion beam showing predicted: Ion distribution (red curve) and vacancy production (blue curve) vs target depth. (For interpretation of the references to colour in this figure legend, the reader is referred to the web version of this article.)